#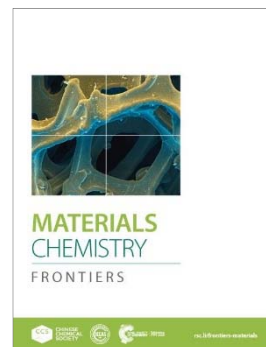 Dye-modified silica-anatase nanoparticles for the ultrasensitive fluorogenic detection of the improvised explosive TATP in an air microfluidic device

SCHOLARONE™
Manuscripts

Research Articles — Referee Guidelines

Research Articles contain **original** scientific work of **high impact** that has not been published previously.

We ask you to only recommend work for publication which demonstrates a significant advance in the field; **routine and incremental** work – however competently researched and reported should **not** be recommended for publication.

Please provide a rapid yet comprehensive evaluation of this work by submitting your report on its **originality**, **significance**, **impact** and **scientific reliability** within **10 days**.

It is the expectation that **only work with two strong endorsements will be accepted** for publication.

Thank you very much for your assistance in reviewing this manuscript.

Materials Chemistry Frontiers
MaterChemFrontiersED@rsc.org

Dear Editor: Please find enclosed the manuscript: Dye-modified silica-anatase nanoparticles for the ultrasensitive fluorogenic detection of the improvised explosive TATP in an air microfluidic device, By: Sindija Lapcinska, Andrea Revilla-Cuesta, Irene Abajo-Cuadrado, José V. Cuevas, Manuel Avella, Pavel Arsenyan and Tomás Torroba, which is intended for publication in the Journal Materials Chemistry Frontiers as a paper. The paper introduces a new material for the detection of traces in air of an important material used in improvised explosive devices, triacetone triperoxide, that constitutes an improvised explosive of very difficult detection, for this reason has been frequently used in suicide terrorist attacks. In this manuscript we introduce the proof of concept of a portable testing setup which will allow for field-testing and generation of real-time results to test for TATP vapor traces in a number of different environments. Our fluorescent methodology is very selective, using recirculation of the gas samples in connection to the sensing mechanism in a suitable microfluidic portable device, allowing for a controlled trapping of triacetone triperoxide in the chemical sensor to give reliable results at very low concentrations in air. Because of the novelty of the reported materials and the interest for the readers of the journal, especially those interested in the detection of traces of improvised explosive devices in air, I think that the paper can be suitable for consideration for publication in the journal as an article.

Dye-modified silica-anatase nanoparticles for the ultrasensitive fluorogenic detection of the improvised explosive TATP in an air microfluidic device

Sindija Lapcinska,[a†] Andrea Revilla-Cuesta,[b†] Irene Abajo-Cuadrado,[b] José V. Cuevas,[b] Manuel Avella,[c] Pavel Arsenyan,*[a] and Tomás Torroba*[b]

We describe the proof of concept of a portable testing setup for the detection of triacetone triperoxide (TATP), a common component in improvised explosive devices, which will allow for field-testing and generation of real-time results to test for TATP vapor traces in a number of different environments, by using recirculation of the gas samples in connection to the sensing mechanism in a suitable microfluidic portable device, allowing for a controlled trapping of the analyte in the chemical sensor to give reliable results at very low concentrations in air

Introduction

The so-called improvised explosive devices (IEDs) are a mayor threat in modern society.[1-6] Explosives commonly used in IEDs have been displaced from war sceneries to everyday life, therefore constituting a nuisance in the lives of several people. Albeit methods for the quick detection of explosive devices are needed, before they cause damage, there are very few methods for the detection of some explosives used in IEDs.[7-11] The foremost advanced spectroscopy devices are indeed sensitive and selective for the purpose of identify this kind of chemicals but they are expensive and usually too heavy for portable devices[12] and the technology of the cotton swab[13] requires physical access to the substance that might be not accessible. The use of animals in the detection of explosives has also a long tradition[14] but for some explosives are less reliable. The electronic noses, constituted by artificial sensors are therefore studied to substitute the natural senses[15-16] on the way to get easy monitorization of different environments. The suitable portable devices should alert of the presence of explosives in a matter of minutes. Triacetone triperoxide (TATP) is straightforwardly synthesized from starting materials of easy access,[17] because of this reason is has been used in IEDs. Albeit TATP sublimes at room temperature, its presence in the vapor phase is not usually detected by the use of common methods for explosives because of the lack of aromatic nitro groups.[18] In contrast, other important explosive, hexamethylene triperoxide diamine (HMTD) also employed in IEDs has a much lower vapor pressure than TATP therefore its detection

in the vapor phase[19] is not possible. Usual methods for the detection of TATP are mass spectrometry,[20] ion mobility spectrometry or related technologies[21-23] and multiphoton spectroscopy.[24] Some alternatives are chemically modified nanosensor arrays,[25] or optical portable methods based on colorimetric sensor arrays that detect hydrogen peroxide (H_2O_2) from TATP decomposition.[26-28] Indirect detection methods, such as detection of H_2O_2 from TATP, linked to oxidative processes, has been used for fluorimetric sensing,[29-31] as well as acetone detection from TATP decomposition.[32-33] Notwithstanding, direct detection of TATP has been achieved by fluorescence quenching.[34] Analytical methods for the detection of TATP (or HMTD) in different scenarios need to be selective for peroxides, suitable for on-site analysis and safe sampling by a specialist,[35] and it is expected to have low limits of detection and high selectivity suitable to check for the peroxides in order to prevent explosions in confined public places.[36] An extremely low limit of detection is easier to achieve with the highly volatile TATP than with the less volatile HMTD.[37] Most physicochemical analytical methods for peroxide-based explosives are designed in this way.[38-39] The detection of traces of TATP in the vapor phase by colorimetric or fluorometric methods by taking in account its volatility is still an attractive approach to the developing of chemical sensors for peroxide explosives. Some characteristics such as sensitivity and selectivity are still not well addressed. Our previous approaches consisted of solid fluorogenic sensors for the sensitive and selective detection of pristine TATP[40-41] and the microwave detection of wet-TATP[42] all in the vapor phase. Looking for more selective and sensitive materials specifically tailored for the unambiguous detection of TATP in the vapor phase,[43] we performed a deep search in our structural diversity of dyes containing selenium[44-46] as the expected fluorescence modulator[47] for the detection of oxidizing species.[48] We selected a coumarin structure for its very good performance in previously known fluorescent chemosensors.[49] By synthetic variations of structural rigidity and substituent position we prepared a new dye with optimum characteristics in which the turn-on fluorescence mechanism could be triggered via oxidation by only

[a.] Latvian Institute of Organic Synthesis, Aizkraukles 21, LV-1006, Riga, Latvia, pavel@osi.lv
[b.] Department of Chemistry, Faculty of Science, University of Burgos, 09001 Burgos, Spain, ttorroba@ubu.es
[c.] Electron Microscopy Lab, IMDEA Materials Institute, Eric Kandel, 2, Tecnogetafe, 28906 Getafe (Madrid), Spain.
† Sindija Lapcinska and Andrea Revilla-Cuesta have contributed equally.
Electronic Supplementary Information (ESI) available: [NMR, HRMS, UV and FL spectra, additional FL and NMR titrations]. See DOI: 10.1039/x0xx00000x

hydrophobic oxygen-containing oxidants. The subsequent study of the dye supported on the surface of silica or anatase nanoparticles should then permit the construction of new materials with optimum performance for the selective and ultrasensitive detection of traces of TATP in a vapor phase. The results of the study are presented here.

Results and discussion

Synthetic procedure

For the synthesis of the fluorogenic dye, the selenyl electrophile was generated from di-*Boc*-seleno-L-cystine by using $K_2S_2O_8$ and then trapped with 2,3,6,7-tetrahydro-1*H*,5*H*-pyrido[3,2,1-ij]quinolin-8-yl 3-phenylpropiolate.[50] Subsequent 6-endo-dig cyclization and reverse phase chromatography provided the required *Boc-Sec* containing coumarin **SL-739** as a brown oil (37%) (Scheme 1).
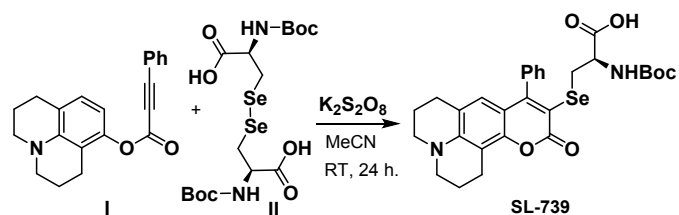
Scheme 1: Synthesis of **SL-739**.

Preparation of modified nanoparticles.

Three types of samples were prepared by adsorption of **SL-739** on commercial nanoparticles to be tested as TATP sensors: (a) silica, (b) anatase and (c) hybrid silica/anatase. Modified silica nanoparticles (**SL-739@SiO$_2$**) were prepared by stirring under nitrogen, in the dark, 1 mg of **SL-739** and 100 mg of silica nanopowder, 10-20 nm particle size, in 5 mL chloroform for 30 minutes until there was no trace of dye in the solvent, then the solvent was evaporated, the solid was washed for three times with hexane (5 mL each), and the solid was subjected to centrifugation and drying under nitrogen stream. Modified titanium(IV) oxide nanoparticles, anatase, (**SL-739@TiO$_2$**) were prepared similarly from 1 mg of **SL-739** and 100 mg of TiO$_2$, anatase nanopowder, <25 nm particle size. Modified titanium silicon oxide (**SL-739@TiSiO$_4$**) were prepared similarly from 1 mg of **SL-739** and 100 mg of TiO$_2$/SiO$_2$ nanopowder, <50 nm particle size (Figure 1).
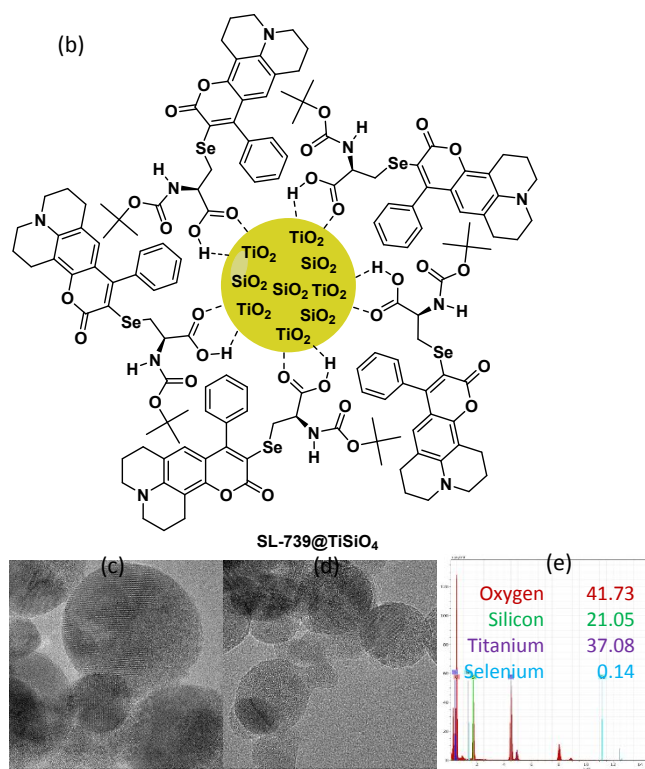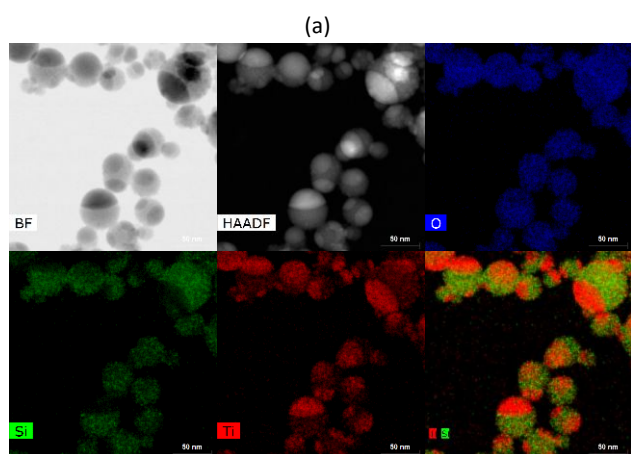
(a)

(b)

SL-739@TiSiO$_4$

Figure 1: (a) Structural and elemental composition of the starting TiSiO$_4$ nanoparticles. (b) Chemical structure representation of **SL-739@TiSiO$_4$**. (c) High resolution TEM image of **SL-739@TiSiO$_4$** as prepared. (d) High resolution TEM image of **SL-739@TiSiO$_4$** after TATP experiments (e) Elemental composition of the **SL-739@TiSiO$_4$** as prepared.

Titrations of SL-739@SiO$_2$/TiO$_2$/TiSiO$_4$ and TATP in the gas phase

We started by checking the fluorescence quantitative changes of solid materials **SL-739@SiO$_2$**, **SL-739@TiO$_2$** and **SL-739@TiSiO$_4$** in the presence of TATP in a vapor flow in a custom-made system as represented in Figure 2. These preliminary experiments employed 2 mg TATP under a dry clean air flow adjusted to 100 cm^3/min in a perforated Eppendorf, gently warmed below 50°C with an external air flow heating (a laboratory hot air gun) (Figure 2e). The gas flow was conducted through a system of two nylon tubes, so recirculation flow is permitted, to another perforated Eppendorf at room temperature containing 15 mg of the required dye-deposited nanoparticles. The air flow diffused through the Eppendorf stoppers to exhaust. The system was maintained under air flow until consumption of TATP in around few seconds to twenty minutes and recirculated for ten more minutes. Then the sensor material was subjected to fluorescence measurements in an Edinburgh Instruments FLS980 fluorometer with solid sample holder. Steady state spectra in all cases showed increase in the emission intensity in the three cases and marked growing of the bands in the region between 400-450 nm, more remarked for **SL-739@TiSiO$_4$** (Figure 2a-d). A consistent comparison of the quantitative increase in fluorescence with the three solid materials was performed by measurement of quantum yield differences between samples, by repeating three times each sample until the error was lower to 2%.

Consequently, for **SL-739@SiO₂** the overall increase of the quantum yield in the presence of TATP vapor was $\Phi_{SL-739@SiO2+TATP}/\Phi_{SL-739@SiO2}$ = 1.20; for **SL-739@TiO₂** the overall increase of the quantum yield in the presence of TATP vapor was $\Phi_{SL-739@TiO2+TATP}/\Phi_{SL-739@TiO2}$ = 1.25; in contrast, for SL-739@TiSiO₄ the overall increase of the quantum yield in the presence of TATP vapor was substantially higher, $\Phi_{SL-739@TiSiO4+TATP}/\Phi_{SL-739@TiSiO4}$ = 2.09, therefore in this case the increase in fluorescence in the presence of TATP vapor was satisfactory for reliable measurements and **SL-739@TiSiO₄** was used exclusively along the rest of the study.
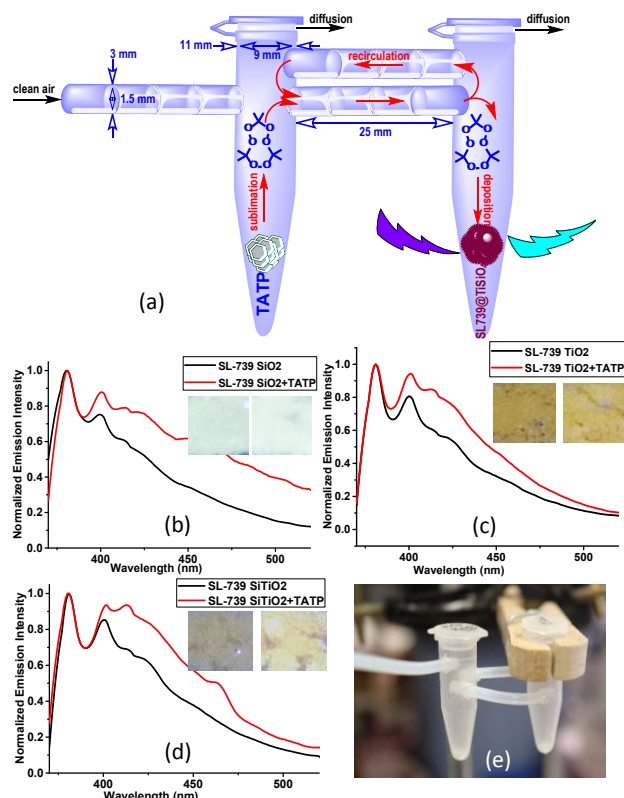

Figure 2: (a) The microfluidic device dimensions: Eppendorf: outer top diameter: 11 mm, inner top diameter: 9 mm, outer bottom diameter: 5 mm, inner bottom diameter: 3 mm, volume: 1.5 mL, height (with lid): 40 mm, height (without lid): 38 mm; tubing: outer diameter: 3 mm, inner diameter: 1.5 mm, length (flow tube): 25 mm, length (return tube:): 35 mm. Normalized fluorescence of (b) **SL-739@SiO₂**, (c) **SL-739@TiO₂**, and (d) **SL-739@SiTiO₄**, pristine (black) and in the presence of excess TATP (red), λ_{exc} = 350 nm. Insets: left: pristine nanoparticles, right: nanoparticles after TATP treatment, all under a UV light 366 nm. (e) The actual aspect of the system.

We then performed a quantitative titration of TATP in the gas phase by using, as previously, batches of 15 mg of **SL-739@SiTiO₄** and increasing amounts of TATP in the microfluidic system maintained under air flow, 100 cm³/min, gently warmed below 50°C until consumption of TATP in every case. The lowest amounts of TATP took only seconds to evaporate (plus ten minutes for recirculation) and the highest amounts took up to twenty minutes, therefore the experiments were performed within ten and thirty minutes until consumption of TATP. Then the sensor material was subjected to fluorescence measurements in every case (Figure 3). The results showed a remarkable sensitivity of **SL-739@SiTiO₄** to very low

amounts of TATP in the vapor phase and a decreased sensitivity at higher amounts of TATP, albeit at even higher amounts of TATP the fluorescence increased steadily.
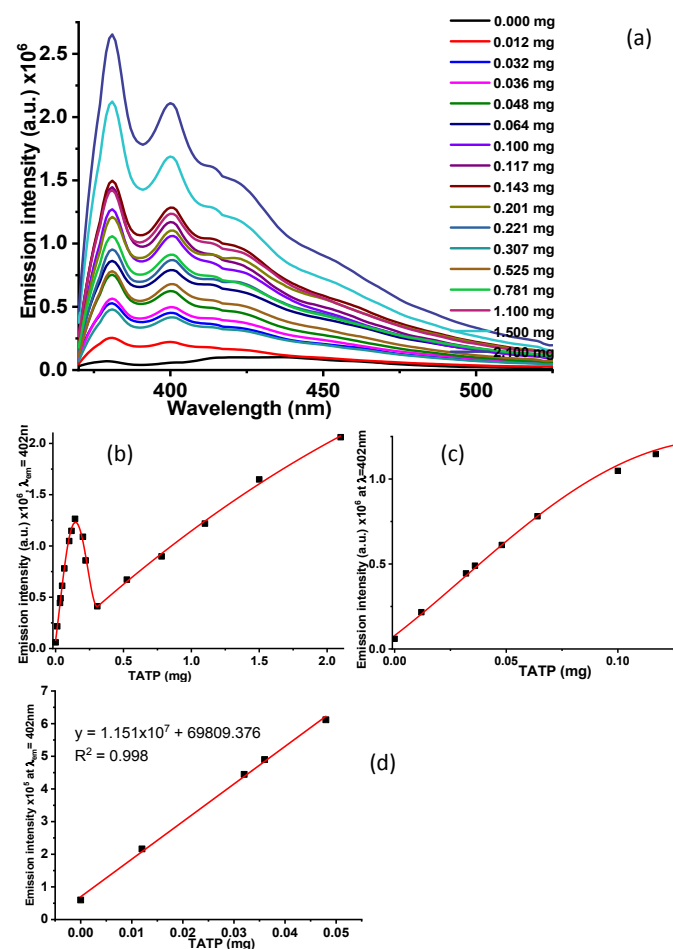

Figure 3: (a) Titration curves of **SL-739@SiTiO₄** with increasing amounts of TATP in the vapor phase. (b) Titration plot of SL-739@SiTiO₄ and increasing amounts of TATP λ_{exc} = 350 nm, λ_{em} = 402 nm. (c) An expansion of the titration plot of **SL-739@SiTiO₄** and increasing amounts of TATP. (d) Linear regression plot at low concentrations of TATP.

The titration plot showed a rapid increase in the fluorescence values under the presence of TATP until a maximum value at 0.14 mg TATP (2.45 equiv), then a decrease from 0.14 to 0.30 mg TATP (5.25 equiv), and then a continuous increase in the fluorescence under increasing amounts of TATP. Therefore, the material works appropriately for the detection of TATP traces in air at concentrations below 0.1 mgL⁻¹ (0.45 μM). We calculated the limits of detection, LODs, from the initial titration plot values by IUPAC-consistent methods.[51] Calculation of the LOD by using a linear regression at low quantities of TATP (LOD = 3.3×SD/s, where SD is the standard deviation of a blank figure sample and s is the slope of the calibration curve in a region of low TATP content) gave a value LOD = 3.3×(325.87861/1.15138×10⁷) = 9.34×10⁻⁵ mg (93.4 ng) in absolute value or, taking in account the time of measurement and air efflux, LOD = 93.4 ngL⁻¹ (0.4 nM). Assuming that the best LOD values are found in the ppb to ppm range for TATP sensing in the gas phase,[52] the explained method competes favorably in terms of sensitivity and simplicity with the known methods with a LOD value of 10 ppb. We

also calculated the LOD within the values measured (different than 0) by adjusting the initial values to a mean square linear regression and using the R program.[53-54] In this way, linear regression at low concentrations of TATP led to a LOD = 5.5 µg in absolute value or, taking in account the time of measurement and air efflux, a LOD = 5.5 µgL^{-1} (24.7 nM), that can be considered as a good approach to the limit of quantification, LOQ, of the material. The maximum saturation equilibrium concentration of TATP has been reported as 600 µgL^{-1} (2.7 µM)[17] therefore, the reported material is well suited for the detection of TATP vapor in a stream flow in the tenths of thousandth of the maximum concentration in air. This unusual behavior in the gas phase was then compared to the study of the dye oxidative behavior by using TATP in solution.

Titrations of SL-739 and TATP or MCPBA in organic solutions

The kinetic study of a 10 µM solution of SL-739 in CHCl$_3$:MeOH 9:1 and a large excess TATP (2 mg in 3 mL solution) showed a slow increase of the fluorescence after the addition of TATP (Figure 4) with appearance first of a band at 540 nm at shorter times of measurements and then of a band centred at 505 nm followed by a shoulder at 460 nm.
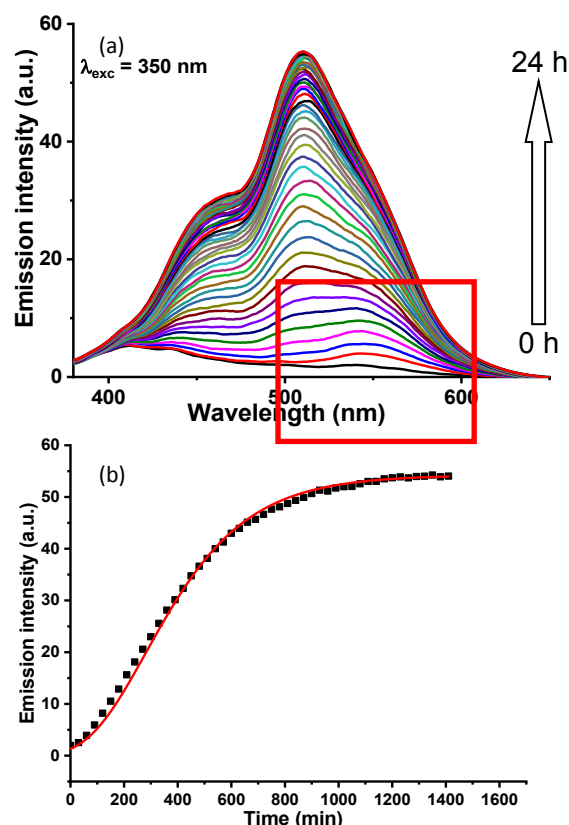

Figure 4: Kinetic study (a) and fluorescence profile as a function of time at 505 nm (b) of a 10 µM solution of **SL-739** in CHCl$_3$:MeOH 9:1 in the presence of excess TATP. Inset: variation of the fluorescence maximum along time.

Point to point titration of 10 µM solutions of **SL-739** in CHCl$_3$:MeOH 9:1, in the presence of increasing amounts of TATP, showed an increase in fluorescence (after one hour for every point) in two different regions at different stages of addition of TATP (Figure 5).

Figure 5: (a) Titration curves of 10 µM solutions of **SL-739** in CHCl$_3$:MeOH 9:1 with increasing amounts of TATP in solution. (b) Titration plots of 10 µM solutions of **SL-739** in CHCl$_3$:MeOH 9:1 with increasing amounts of TATP in solution, λ$_{exc}$ = 350 nm, λ$_{em}$ = 413, 435 and 547 nm. (c) Ratiometric plots of different emission bands, 413/547, 435/547, 547/413 and 547/435. (d) Linear regression plot at low concentrations of TATP of the ratiometric factor 413/547.

First, two bands at 413 and 435 nm grew steadily until 50 µM solution TATP was added and then decreased until 100 µM TATP and then

somewhat increased under higher amounts of TATP. When the bands at 413 and 435 nm decreased to a minimum, a band at 547 nm started to grow steadily until the end of titration, a similar behaviour of the emission band found in the kinetics experiment under similar time of measurement. Ratiometric plots of the different emission bands, 413/547, 435/547, 547/413 and 547/435 at low concentrations of TATP showed patterns of increase or decrease of ratios until 50 µM solution TATP was added, then patterns are reversed until 100 µM TATP solution, then increase and decrease are again reversed until 1mM TATP solution and a confluence point at 3 mM TATP, where all ratios have similar values, is reached, after that 547/413 and 547/435 ratios grew steadily and 413/547 and 435/547 ratios decreased steadily until the end of titration. We calculated the LOD within the values measured (different than 0) by adjusting the initial values of the ratiometric factor 413/547 to a mean square linear regression and using the R program.[53-54] In this case, the linear regression at low concentrations of TATP led to a limit of detection of 2.8 µM TATP, that can be considered as a good approach to the limit of quantification, LOQ, of the material, and it is suitable for practical purposes. Remarkably, under low amounts of TATP only bands around 400 nm are shown, as in the case of the experiments in the gas phase, where the concentration of TATP in air is limited to the saturation equilibrium concentration. The slow kinetics of increase of fluorescence showed by **SL-739** in the presence of TATP in solution was in strong contrast to the rapid kinetics in the behavior shown by **SL-739@SiTiO₄** and TATP vapor. Apparently, the supporting nanoparticles accelerated the reaction by catalyzing the expected oxidation process. To complement the study, we then used a classic oxidant, *meta*-chloroperbenzoic acid (MCPBA) for kinetic studies and titration experiments with **SL-739** in solution. Under the kinetics experiment, addition of MCPBA excess to **SL-739**, 2.5 µM in CHCl₃:MeOH 9:1, showed a rapid increase of the fluorescence value at 445 and then increased very little on time (Figure 5).

Figure 6: Kinetic study (a) and fluorescence profile as a function of time at 445 nm (b) of a solution of **SL-739**, 2.5 µM in CHCl₃:MeOH 9:1, in the presence of excess MCPBA (2 mg in 3 mL).

Therefore, the titration experiment was performed in one single fluorescence cell, by successive additions of MCPBA. Titration of a **SL-739** solution, 2.5 µM in CHCl₃:MeOH 9:1, under increasing concentrations of MCPBA, is shown in Figure 7.
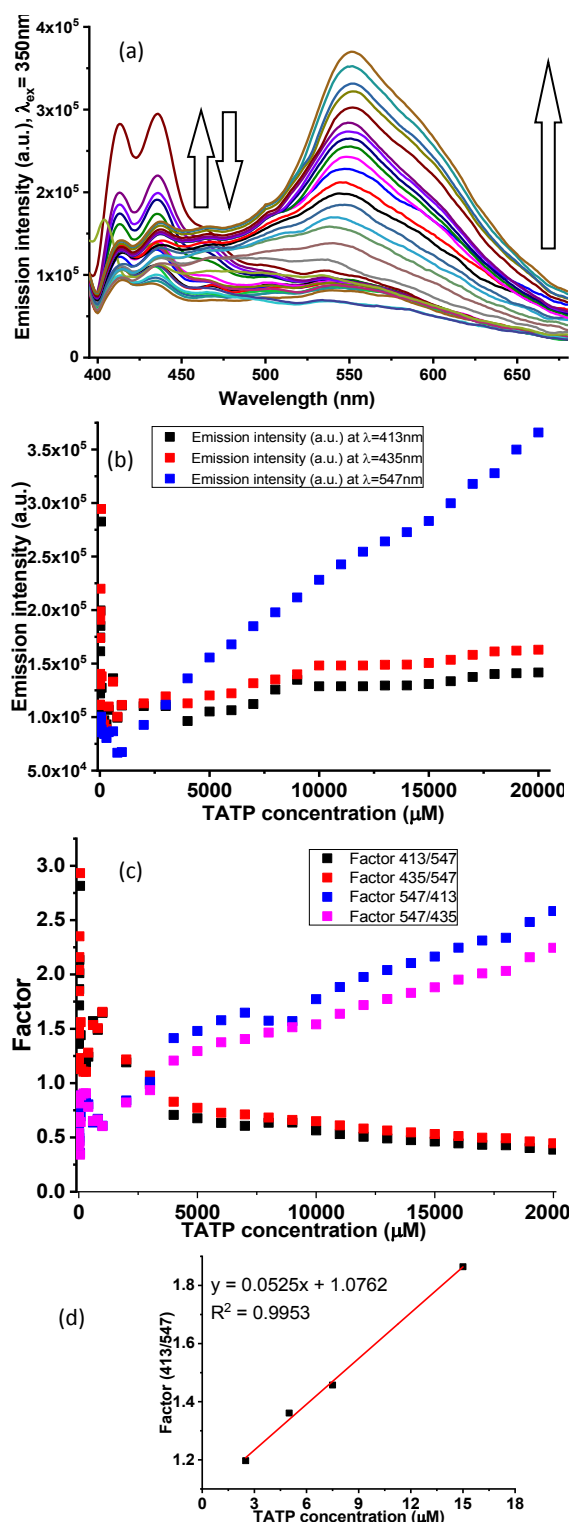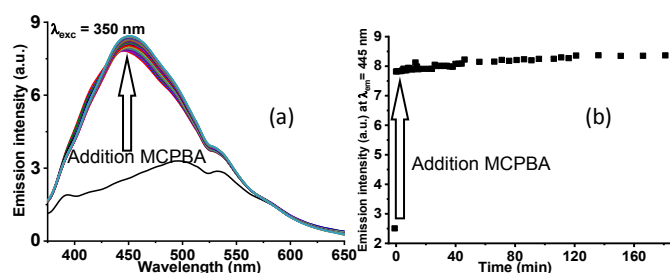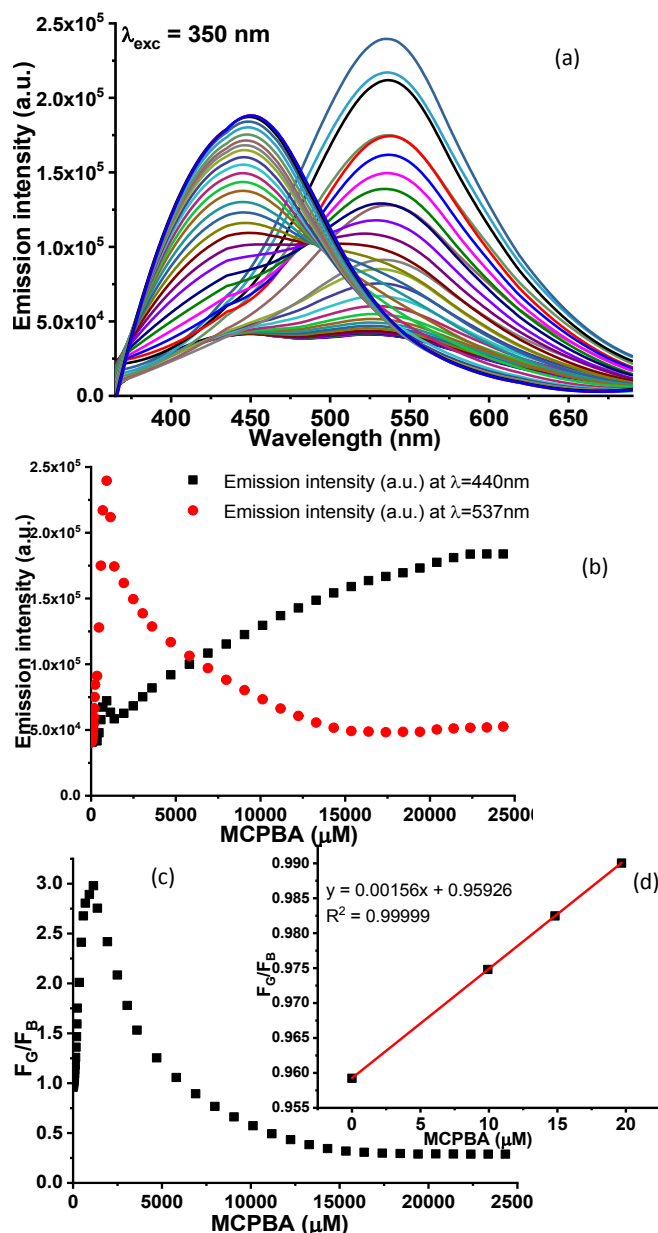

Figure 7: (a) Titration curves of 2.5 µM solutions of **SL-739** in CHCl₃:MeOH 9:1 with increasing amounts of MCPBA in solution. (b) Combined titration plots 2.5 µM solutions of SL-739 in CHCl₃:MeOH 9:1 with increasing amounts of MCPBA in solution, λ_{exc} = 350 nm, λ_{em} = 440 and 537 nm. (c) Ratiometric plot of the two emission bands, 537/440. (d) Linear regression plot at low concentrations of TATP of the ratiometric factor F_g/F_b.

The titration curves showed two emission peaks at 440 nm and 537 nm under a wavelength excitation of 350 nm. With the addition of MCPBA, the intensity of the green emission at 537 nm (Fg) first quickly increased until a maximum at 920 µM MCPBA and then gradually decreased as a blue emission at 440 nm (Fb) steadily increased and remained until the end of titration, apparently the same band shown during the kinetics experiment under excess MCPBA. The ratio of fluorescence intensities at 537 and 440 nm (Fg/Fb) exhibited a sharp increase of value until 1.15 mM MCPBA and then asymptotically decreased with increasing MCPBA concentrations. For completeness we also calculated the LOD within

the values measured (different than 0) by adjusting the initial values of the ratiometric factor 537/440 to a mean square linear regression and using the R program.[53-54] In this case, the linear regression at low concentrations of MCPBA led to a limit of detection of 0.18 µM MCPBA, lower than in the case of TATP in solution, that can be considered as a good approach to the limit of quantification, LOQ, of the material. MCPBA is not a species searched in environmental samples, therefore the obtained values constituted only a reference of the sensitivity of the probe.

Qualitative interferents tests

Previous experiments had already shown the selectivity of the **SL-739** probe to the presence of oxidants such as TATP or MCPBA exclusively. Addition of excess common anions or cations did not show changes in color or fluorescence, only excess gold(III), as hydrogen tetrachloroaurate(III), showed a neat increase of fluorescence (See the Supporting Information). In contrast to probes with large selection of analytes,[55] **SL-739** probe was not sensitive to the presence of nitrated explosives such as trinitrobenzene (TNB) or trinitrotoluene (TNT) or common oxidants such as hydrogen peroxide or nitric acid in the conditions performed for the qualitative experiments, following related conditions to the previously used for titration experiments. Thus, 25 µM solutions of **SL-739** in $CHCl_3$:MeOH 9:1, in the presence of increasing amounts of analytes and suspected interferents, were left for one hour and then taken photographs under a 366 nm UV light. In some instances, large excess reagents or suspected interferents are added to guarantee that there is no interference. It is remarkable the different response to TATP or MCPBA and the absence of response to the presence of excess hexamethylene triperoxide diamine (HMTD) (Figure 8).
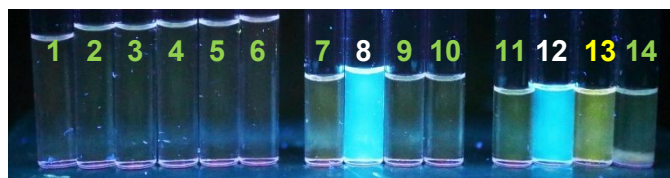

Figure 8: Qualitative experiments of sensitivity of **SL-739**, showing the different response given to acids, oxidizing and reducing reagents, nitrated explosives, and peroxide explosives: [1] Ref: **SL-739**, 20 µM in $CHCl_3$:MeOH 9:1, 500 µL, + 400 µL MeOH, [2] Ref[1]+8 equiv HCl 0.5 mM in 160 µL H_2O + 400 µL MeOH, [3] Ref[1]+8 equiv HNO_3 0.5 mM in 160 µL H_2O + 400 µL MeOH. [4] Ref[1]+8 equiv oxone 0.5 mM in 160 µL H_2O + 400 µL MeOH, [5] Ref[1]+8 equiv hydrazine 0.5 mM in 160 µL H_2O + 400 µL MeOH, [6] Ref[1]+8 equiv hydrogen peroxide 0.5 mM in 160 µL H_2O + 50 µL hydrogen peroxide, 30% w/w in water, + 400 µL MeOH, [7] Ref: SL-739, 20 µM in $CHCl_3$:MeOH 9:1, 500 µL + 160 µL MeOH, [8] Ref[7]+8 equiv MCPBA 0.5 mM in 160 µL MeOH+2 mg solid MCPBA, [9] Ref[7] + 8 equiv TNB 0.5 mM in 160 µL MeOH, [10] Ref[7] + 8 equiv TNT 0.5 mM in 160 µL MeOH, [11] Ref: SL-739, 20 µM in $CHCl_3$:MeOH 9:1, 500 µL, [12] Ref[11] + 2 mg MCPBA, [13] Ref[11] + 2 mg TATP, [14] Ref[11] + 2 mg HMTD, photograph under 366 nm UV light, taken 1 h after the last addition.

DFT Calculations

The non-linear behavior of the **SL-739** probe, either in solution or supported on $TiSiO_4$ hybrid nanoparticles, was certainly unexpected, giving a different performance at different concentrations of oxidants. We reasoned that different oxidation states of the

molecule could give different emission spectra. Being intermediate species in the titration experiments, calculation of the different species in the titration process could be a way to understand the fluorescence changes. For this purpose, DFT and TD-DFT calculations were carried out in order to understand the photophysical behavior observed. The oxidation of **SL-739** (**1**) can lead to the formation of the products **2** and **3** (Figure 9). All species have been modeled in their ground state and the calculated values of the gap HOMO-LUMO were 3.46, 3.47 and 3.42 eV for the species **1** to **3** respectively. TD-DFT calculations were performed to estimate the excitation energy of these molecules as the value of the energy of the first excited state calculated with the geometry of the ground state. The values obtained for these energies of excitation were 391.6, 397.2 and 392.9 nm for the species **1** to **3** respectively. The emission values were estimated as the difference in energy between the first singlet excited state and the ground state for each model. The calculated value for **1**, **2** and **3** were 537.6, 576.8 and 458.0 nm respectively. The value of the mono-oxidized molecule **2** (576.8 nm) is in good agreement with the experimentally observed emission at 537 nm. This band vanished after an initial sharp growing, meanwhile the signal appearing at 440 nm was growing in intensity. The experimental signal at 440 nm can be correlated to the theoretical signal at 458.0 nm that belonged to the emission from the S_1 excited state to the S_0 of the selenodioxide model 3 (Table 1).
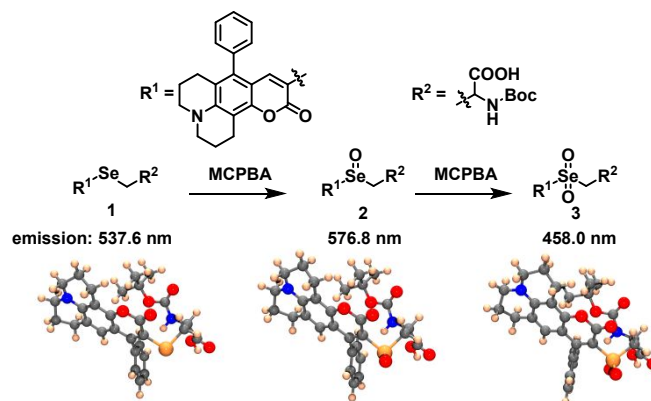

Figure 9: Models of oxidation intermediates employed for the DFT calculations of emission wavelengths.

Table 1. Calculated maximum absorption and emission wavelength of modeled species at the B3LYP/def2-svp level of theory with the SMD solvation model (chloroform).

Molecule	Items	λ (nm; eV)
1	Absorption	391.6; 3.17
	Emission	537.6; 2.31
2	Absorption	397.2; 3.12
	Emission	576.8; 2.15
3	Absorption	392.9; 3.16
	Emission	458.0; 2.71

We also calculated the interaction of the carboxylate moiety with the solid TiO_2 with anatase structure through the facet (100), that was modeled at the semiempirical level PM6. As expected, both oxygen atoms of the carboxylate were orientated towards two titanium atoms of the anatase with distances of 2.350 and 2.478 Å. The substituents of the α-carbon of the amino acid displayed a disposition in which the amino fragment and the selenium were

orientated away from the TiO$_2$, being the plane of coumarin fragment almost perpendicular to the facet (100) of the anatase (with an angle of 83.02°) (Figure 10).
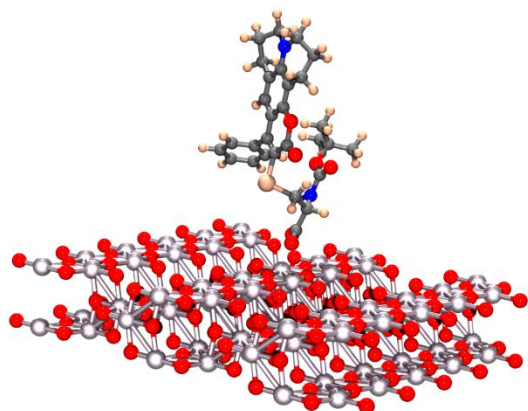

Figure 10: Model of interaction of the carboxylate moiety of SL-739 with the solid TiO$_2$ with anatase structure through the facet (100).

For completeness of the mechanistic experiments, we performed ^{1}H-NMR titration experiments of **SL-739** (3 mg **SL-739** in 0.5 mL CDCl$_3$ as solvent) with increasing amounts of TATP (from 5 µg to 15.8 mg) or MCPBA (from 5 µg to 3.2 mg) (See the Supporting Information). We did not notice large changes in the ^{1}H-NMR spectra, other than the opposite displacement of the OH proton signal due to the different environments of each titration, and some desymmetrization in the aliphatic signals, which in summary is compatible with the stepwise oxidation of the selenium atom along the titration experiments with TATP or MCPBA.[56]

Experimental

Synthesis of SL-739. 2,3,6,7-Tetrahydro-1*H*,5*H*-pyrido[3,2,1-*ij*]quinolin-8-yl 3-phenylpropiolate (I) (83 mg, 0.22 mmol, 1.4 equiv.) and K$_2$S$_2$O$_8$ (2.53 g, 9.4 mmol, 50 equiv.) were added to a solution of di-*Boc*-seleno-L-cystine (II) (100 mg, 0.187 mmol, 1 equiv.) in MeCN (5 ml). The reaction mixture was stirred until disappearance of starting materials, filtrated, evaporated and purified by reverse phase chromatography (C-18, MeCN/H$_2$O+AcOH 20-85%) to provide product SL-739 as a brown oil (40 mg, 37%) (Scheme 1). [α]$_D^{20}$ = -34.7 (c 0.73, MeOH). ^{1}H NMR (400 MHz, CD$_3$OD) δ = 7.70–7.60 (m, 2H), 7.60–7.50 (m, 1H), 7.50–7.41 (m, 2H), 7.11 (s, 1H), 4.30–4.24 (m, 1H), 3.21–3.12 (m, 5H), 2.95 (dd, *J* = 12.5, 8.3 Hz, 1H), 2.77–2.69 (m, 2H), 2.63–2.55 (m, 2H), 1.98–1.89 (m, 4H), 1.41 (s, 9H). ^{13}C NMR (101 MHz, CD$_3$OD) δ = 174.5, 157.6, 153.4, 149.7, 146.0, 136.2, 134.3, 132.3, 130.0, 121.7, 120.5, 115.3, 106.7, 89.3, 81.1, 80.5, 50.8, 50.2, 40.9, 30.9, 28.7, 28.4, 23.4, 22.8, 22.2. ^{77}Se NMR (76 MHz, CD$_3$OD) δ = 195.1. HRMS (ESI/Q-TOF) m/z: [M+Na]$^+$ calcd for [C$_{29}$H$_{32}$N$_2$O$_6$SeNa]$^+$ 607.1323; found 607.1324. [M]$^+$ calcd for [C$_{29}$H$_{32}$N$_2$O$_6$Se]$^+$ 584.1426; found 584.1426.

DFT Calculations. The geometry optimization of **SL-739** and the products of its oxidation both in the ground state and the singlet first excited state were carried out using the ORCA software.[57-58] The singlet ground state (S$_0$) geometries in them were optimized using

DFT calculations with the Becke-3-Lee–Yang–Parr (B3LYP) functional[59-60] and def2-SVP basis set.[61] The electronic absorptions and the geometries of the lowest singlet excited state (S$_1$) were optimized by using Time Dependent-DFT (TD-DFT) at the same level of theory. The solvation effects were considered using the continuum model SMD.[62] The data of emission energies were estimated as the difference of energy between the S$_1$ and S$_0$ structures. The interaction of SL-739 with the plane 100 of anatase was modeled at the semiempirical PM6 level of theory[63] as using the Gaussian 09 software package,[64] without any restriction imposed to SL-739, but freezing the atoms of the anatase to simulate a solid particle.

Conclusions

Triacetone triperoxide (TATP) constitutes an improvised explosive of very difficult detection, for this reason has been frequently used in suicide terrorist attacks. The proof of concept of a portable testing setup was developed which will allow for field-testing and generation of real-time results to test for TATP vapor traces in a number of different environments. Our fluorescent methodology is very selective, using recirculation of the gas samples in connection to the sensing mechanism in a suitable microfluidic portable device, allowing for a controlled trapping of analyte in the chemical sensor to give reliable results at very low concentrations in air.

Author Contributions

Sindija Lapcinska performed the synthesis, purification and characterization of **SL-739**, Andrea Revilla-Cuesta performed the titration experiments in the gas phase, Irene Abajo-Cuadrado performed the experiments in solution and the formal analysis of the data, José V. Cuevas performed the DFT experiments, Manuel Avella performed the high resolution TEM experiments, Pavel Arsenyan and Tomás Torroba performed supervision, writing the original draft, review and editing of the manuscript.

Conflicts of interest

There are no conflicts to declare.

Acknowledgements

References

1   Improvised Explosive Devices - Past, Present and Future, Action on Armed Violence, 15 Oct 2020, [https://reliefweb.int/report/world/improvised-explosive-devices-past-present-and-future] accessed 05/04/2021.

2   IED Attack, Improvised Explosive Devices, National Academies and the Department of Homeland Security, Dec. 15, 2020, [https://www.dhs.gov/xlibrary/assets/prep_ied_fact_sheet.pdf] accessed 05/04/2021.

3   Reducing the Threat of Improvised Explosive Device Attacks by Restricting Access to Explosive Precursor Chemicals, National Academies of Sciences, Engineering, and Medicine, 2018, The National Academies Press, Washington, DC, DOI: 10.17226/24862.

4   Improvised Explosive Device (IED) Guidelines for Crowded Places, Commonwealth of Australia 2017, ISBN: 978-1-925593-95-2.

5   United Nations Mine Action Service - Improvised Explosive Device Lexicon, [https://unmas.org/sites/default/files/unmas_ied_lexicon_0.pdf] accessed 05/04/2021.

6   European Union Terrorism Situation and Trend Report 2019, European Union Agency for Law Enforcement Cooperation, 2019, DOI: 10.2813/788404.

7   K. C. To, S. Ben-Jaber and I. P. Parkin, Recent Developments in the Field of Explosive Trace Detection, *ACS Nano*, 2020, **14**, 10804–10833.

8   T. Wasilewski and J. Gębicki, Emerging strategies for enhancing detection of explosives by artificial olfaction, *Microchem. J.*, 2021, **164**, 106025.

9   T. P. Forbes, S. T. Krauss and G. Gillen, Trace detection and chemical analysis of homemade fuel-oxidizer mixture explosives: Emerging challenges and perspectives, *Trends Anal. Chem.*, 2020, **131**, 116023.

10 R. Liu, Z. Li, Z. Huang, K. Li and Y. Lv, Biosensors for explosives: State of art and future trends, *Trends Anal. Chem.*, 2019, **118**, 123-137.

11 R. Apak, S. D. Çekiç, A. Uzer, E. Çapanoglu, S. E. Çelik, M. Bener, Z. Can and S. Durmazel, Colorimetric sensors and nanoprobes for characterizing antioxidant and energetic substances, *Anal. Methods*, 2020, **12**, 5266-5321.

12 A. Ostrinskaya, R. R. Kunz, M. Clark, R. P. Kingsborough, T.-H. Ong and S. Deneault, Rapid Quantitative Analysis of Multiple Explosive Compound Classes on a Single Instrument via Flow-Injection Analysis Tandem Mass Spectrometry, *J. Forensic Sci.*, 2019, **64**, 223-230.

13 J. M. E. Glackin, R. N. Gillanders, F. Eriksson, M. Fjällgren, J. Engblom, S. Mohammed, I. D. W. Samuel and G. A. Turnbull, Explosives detection by swabbing for improvised explosive devices, *Analyst*, 2020, **145**, 7956–7963.

14 T.-H. Ong, T. Mendum, G. Geurtsen, J. Kelley, A. Ostrinskaya and R. Kunz, Use of Mass Spectrometric Vapor Analysis To Improve Canine Explosive Detection Efficiency, *Anal. Chem.*, 2017, **89**, 6482–6490.

15 Z. Li, J. R. Askim and K. S. Suslick, The Optoelectronic Nose: Colorimetric and Fluorometric Sensor Arrays, *Chem. Rev.*, 2019, **119**, 231–292.

16 Z. Li and K. S. Suslick, The Optoelectronic Nose, *Acc. Chem. Res.*, 2021, **54**, 950–960.

17 M. A. C. Härtel, T. M. Klapötke, B. Stiasny and J. Stierstorfer, Gas-phase Concentration of Triacetone Triperoxide (TATP) and Diacetone Diperoxide (DADP), *Propellants Explos. Pyrotech.*, 2017, **42**, 623–634

18 F. Dubnikova, R. Kosloff, J. Almog, Y. Zeiri, R. Boese, H. Itzhaky, A. Alt and E. Keinan, Decomposition of Triacetone Triperoxide Is an Entropic Explosion, *J. Am. Chem. Soc.*, 2005, **127**, 1146-1159.

19 K. Colizza, A. Yevdokimov, L. McLennan, J. L. Smith and J. C. Oxley, Using Gas Phase Reactions of Hexamethylene Triperoxide Diamine (HMTD) to Improve Detection in Mass Spectrometry, *J. Am. Soc. Mass Spectrom.*, 2018, **29**, 675-684.

20 M. Makinen, M. Nousiainen and M. Sillanpaa, Ion spectrometric detection technologies for ultra-traces of explosives: A review, *Mass Spectrom. Rev.*, 2011, **30**, 940-973.

21 D. Jiang, L. Peng, M. Wen, Q. Zhou, C. Chen, X. Wang, W. Chen and H. Li, Dopant-Assisted Positive Photoionization Ion Mobility Spectrometry Coupled with Time-Resolved Thermal Desorption for On-Site Detection of Triacetone Triperoxide and Hexamethylene Trioxide Diamine in Complex Matrices, *Anal. Chem.*, 2016, **88**, 4391–4399.

22 D. N. Correa, J. J. Melendez-Perez, J. J. Zacca, R. Borges, E. M. Schmidt, M. N. Eberlin and E. C. Meurer, Direct Detection of Triacetone Triperoxide (TATP) in Real Banknotes from ATM Explosion by EASI-MS, *Propellants Explos. Pyrotech.*, 2017, **42**, 370–375.

23 S. Hagenhoff, J. Franzke and H. Hayen, Determination of Peroxide Explosive TATP and Related Compounds by Dielectric Barrier Discharge Ionization-Mass Spectrometry (DBDI-MS), *Anal. Chem.*, 2017, **89**, 4210–4215.

24 S. Tang, N. Vinerot, D. Fisher, V. Bulatov, Y. Yavetz-Chen and I. Schechter, Detection and mapping of trace explosives on surfaces under ambient conditions using multiphoton electron extraction spectroscopy (MEES), *Talanta*, 2016, **155**, 235–244.

25 A. Lichtenstein, E. Havivi, R. Shacham, E. Hahamy, R. Leibovich, A. Pevzner, V. Krivitsky, G. Davivi, I. Presman, R. Elnathan, Y. Engel, E. Flaxer and F. Patolsky, Supersensitive fingerprinting of explosives by chemically modified nanosensors arrays, *Nat. Commun.*, 2014, **5**, 4195.

26 H. Lin and K. S. Suslick, A Colorimetric Sensor Array for Detection of Triacetone Triperoxide Vapor, *J. Am. Chem. Soc.*, 2010, **132**, 15519–15521.

27 Z. Li, W. P. Bassett, J. R. Askim and K. S. Suslick, Differentiation among peroxide explosives with an optoelectronic nose, *Chem. Commun.*, 2015, **51**, 15312–15315.

28 J. R. Askim, Z. Li, M. K. LaGasse, J. M. Rankin and K. S. Suslick, An optoelectronic nose for identification of explosives, *Chem. Sci.*, 2016, **7**, 199–206.

29 M. Xu, J.-M. Han, C. Wang, X. Yang, J. Pei and L. Zang, Fluorescence Ratiometric Sensor for Trace Vapor Detection of Hydrogen Peroxide, *ACS Appl. Mater. Interfaces*, 2014, **6**, 8708-8714.

30 Q.-H. Zhu, G.-H. Zhang, W.-L. Yuan, S.-L. Wang, L. He, F. Yong and G.-H. Tao, Handy fluorescent paper device based on a curcumin derivative for ultrafast detection of peroxide-based explosives, *Chem. Commun.*, 2019, **55**, 13661-13664.

31 X. Yu, Y. Gong, W. Xiong, M. Li, J. Zhao and Y. Che, Turn-on Fluorescent Detection of Hydrogen Peroxide and Triacetone Triperoxide via Enhancing Interfacial Interactions of a Blended System, *Anal. Chem.*, 2019, **91**, 6967–6970.

32 Y. Qi, W. Xu, N. Ding, X. Chang, C. Shang, H. Peng, T. Liu and Y. Fang, A film-based fluorescent device for vapor phase detection of acetone and related peroxide explosives, *Mater. Chem. Front.*, 2019, **3**, 1218-1224.

33 Y. An, X. Xu, K. Liu, X. An, C. Shang, G. Wang, T. Liu, H. Li, H. Peng and Y. Fang, Fast, sensitive, selective and reversible fluorescence monitoring of TATP in a vapor phase, *Chem. Commun.*, 2019, **55**, 941-944.

34 M. R. Rao, Y. Fang, S. De Feyter and D. F. Perepichka, Conjugated Covalent Organic Frameworks via Michael Addition–Elimination, *J. Am. Chem. Soc.*, 2017, **139**, 2421–2427.

35 K. Liu, Z. Wang, C. Shang, X. Li, H. Peng, R. Miao, L. Ding, J. Liu, T. Liu and Y. Fang, Unambiguous Discrimination and Detection

of Controlled Chemical Vapors by a Film-Based Fluorescent Sensor Array, *Adv. Mater. Technol.*, 2019, **4**, 1800644.

36 Analysis of Explosives Reference List, OSAC, 2020, https://www.nist.gov/system/files/documents/2020/03/27/OSAC%20-%20Explosives%20References%20List%20Feb%-2019%202020.pdf, accessed 05/04/2021.

37 Characteristics of Improvised Explosive Devices containing chemical substances in the context of the international airports protection, EU-SENSE, 2021, https://eu-sense.eu/characteristics-of-improvised-explosive-devices-containing-chemical-substances-in-the-context-of-the-international-airports-protection/, accessed 05/04/2021.

38 A. González-Calabuig, X. Cetó and M. del Valle, Electronic tongue for nitro and peroxide explosive sensing, *Talanta*, 2016, **153**, 340–346.

39 V. Krivitsky, B. Filanovsky, V. Naddaka and F. Patolsky, Direct and Selective Electrochemical Vapor Trace Detection of Organic Peroxide Explosives via Surface Decoration, *Anal. Chem.*, 2019, **91**, 5323–5330.

40 P. Calvo-Gredilla, J. García-Calvo, J. V. Cuevas, T. Torroba, J.-L. Pablos, F. C. García, J.-M. García, N. Zink-Lorre, E. Font-Sanchis, A. Sastre-Santos and F. Fernández-Lázaro, Solvent-Free Off–On Detection of the Improvised Explosive Triacetone Triperoxide (TATP) with Fluorogenic Materials, *Chem. Eur. J.*, 2017, **23**, 13973–13979.

41 J. García-Calvo, P. Calvo-Gredilla, M. Ibáñez-Llorente, D. C. Romero, J. V. Cuevas, G. García-Herbosa, M. Avella and T. Torroba, Surface functionalized silica nanoparticles for the off–on fluorogenic detection of an improvised explosive, TATP, in a vapour flow, *J. Mater. Chem. A*, 2018, **6**, 4416-4423.

42 S. Blanco, A. Macario, J. García-Calvo, A. Revilla-Cuesta, T. Torroba and J. C. López, Microwave Detection of Wet Triacetone Triperoxide (TATP): Non-Covalent Forces and Water Dynamics, *Chem. Eur. J.*, 2021, **27**, 1680-1687.

43 T. Torroba, I. Schechter, J. G. Calvo and A. Revilla-Cuesta, Multi-Year Project: Development of New Chemical Sensors and Optical Technologies for Fast and Sensitive Detection of Improvised Explosives, NATO Science for Peace and Security Series-B: Physics and Biophysics: Explosives Detection, Sensors, Electronic Systems and Data Processing, L. Capineri and E. K. Turmus, Eds., Springer, The Netherlands, 2019, pp. 208-247.

44 A. Ivanova and P. Arsenyan, Rise of diselenides: Recent advances in the synthesis of heteroarylselenides, *Coord. Chem. Rev.*, 2018, **370**, 55–68.

45 P. Arsenyan, S. Lapcinska, A. Ivanova and J. Vasiljeva, Peptide Functionalization Through the Generation of Selenocysteine Electrophile, *Eur. J. Org. Chem.*, 2019, 4951-4961.

46 S. Lapcinska and P. Arsenyan, Selenocystine Peptides Performance in 5-endo-dig Reactions, *Eur. J. Org. Chem.*, 2020, 784-795.

47 A. Abdillah, P. M. Sonawane, D. Kim, D. Mametov, S. Shimodaira, Y. Park and D. G. Churchill, Discussions of Fluorescence in Selenium Chemistry: Recently Reported Probes, Particles, and a Clearer Biological Knowledge, *Molecules*, 2021, **26**, 692.

48 D. Pham, U. Basu, I. Pohorilets, C. M. St Croix, S. C. Watkins and K. Koide, Fluorogenic Probe Using a Mislow–Evans Rearrangement for Real-Time Imaging of Hydrogen Peroxide, *Angew. Chem. Int. Ed.*, 2020, **59**, 17435–17441.

49 D. Cao, Z. Liu, P. Verwilst, S. Koo, P. Jangjili, J. S. Kim and W. Lin, Coumarin-Based Small-Molecule Fluorescent Chemosensors, *Chem. Rev.*, 2019, **119**, 10403–10519.

50 Y. Yang, B. Bai, M. Jin, Z. Xu, J. Zhang, W. Li, W. Xu, X. Wang and C. Yin, Fluorescent imaging of Au3+ in living cells with two new high selective Au3+ probes, *Biosens. Bioelectron.*, 2016, **86**, 939-943.

51 F. Allegrini and A. C. Olivieri, IUPAC-Consistent Approach to the Limit of Detection in Partial Least-Squares Calibration, *Anal. Chem.*, 2014, **86**, 7858–7866.

52 J. H. Fujiyama-Novak, C. K. Gaddam, D. Das, R. L. V. Wal and B. Ward, Detection of explosives by plasma optical emission spectroscopy, *Sens. Actuators B*, 2013, **176**, 985–993.

53 M. C. Ortiz, L. A. Sarabia and M. S. Sánchez, Tutorial on evaluation of type I and type II errors in chemical analyses: From the analytical detection to authentication of products and process control, *Anal. Chim. Acta*, 2010, **674**, 123-142.

54 RStudio, Version 1.4.1103, 2009-2021 RStudio, 250 Northern Ave, Boston, MA 02210.

55 P. Zheng, A. Abdurahman, Z. Zhang, Y. Feng, Y. Zhang, X. Ai, F. Li and M. Zhang, A simple organic multi-analyte fluorescent prober: One molecule realizes the detection to DNT, TATP and Sarin substitute gas, *J. Hazard. Mater.*, 2021, **409**, 124500.

56 J. Drabowicz, J. Lewkowski and J. Scianowski, Selenium Compounds with Valency Higher than Two, in: Organoselenium Chemistry: Synthesis and Reactions, T. Wirth, Ed., 2012, Wiley-VCH, Weinheim, Germany, Chapt. 5, pp. 191-256. DOI: 10.1002/9783527641949.

57 F. Neese, The ORCA Program System, WIREs Comput. Mol. Sci., 2012, 2, 73–78. https://doi.org/10.1002/wcms.81.

58 F. Neese, Software Update: The ORCA Program System, Version 4.0. *WIREs Comput. Mol. Sci.*, 2018, **8**, e1327.

59 A. D. Becke, Density-Functional Thermochemistry. III. The Role of Exact Exchange, *J. Chem. Phys.*, 1993, **98**, 5648–5652.

60 C. T. Lee, W. T. Yang and R. G. Parr, Development of the Colle-Salvetti Correlation-Energy Formula into a Functional of the Electron-Density, *Phys. Rev. B*, 1988, **37**, 785–789.

61 F. Weigend and R. Ahlrichs, Balanced Basis Sets of Split Valence, Triple Zeta Valence and Quadruple Zeta Valence Quality for H to Rn: Design and Assessment of Accuracy, *Phys. Chem. Chem. Phys.* 2005, **7**, 3297–3305.

62 A. V. Marenich, C. J. Cramer and D. G. Truhlar, Universal Solvation Model Based on Solute Electron Density and on a Continuum Model of the Solvent Defined by the Bulk Dielectric Constant and Atomic Surface Tensions, *J. Phys. Chem. B*, 2009, **113**, 6378–6396.

63 J. J. P. Stewart, Optimization of Parameters for Semiempirical Methods V: Modification of NDDO Approximations and Application to 70 Elements, *J. Mol. Model.*, 2007, **13**, 1173–1213.

64 M. J. Frisch, G. W. Trucks, H. B. Schlegel, G. E. Scuseria, M. A. Robb, J. R. Cheeseman, G. Scalmani, V. Barone, B. Mennucci, G. A. Petersson, H. Nakatsuji, M. Caricato, X. Li, H. P. Hratchian, A. F. Izmaylov, J. Bloino, G. Zheng, J. L. Sonnenberg, M. Hada, M. Ehara, K. Toyota, R. Fukuda, J. Hasegawa, M. Ishida, T. Nakajima, Y. Honda, O. Kitao, H. Nakai, T. Vreven, J. A. Montgomery, Jr., J. E. Peralta, F. Ogliaro, M. Bearpark, J. J. Heyd, E. Brothers, K. N. Kudin, V. N. Staroverov, T. Keith, R. Kobayashi, J. Normand, K. Raghavachari, A. Rendell, J. C. Burant, S. S. Iyengar, J. Tomasi, M. Cossi, N. Rega, J. M. Millam, M. Klene, J. E. Knox, J. B. Cross, V. Bakken, C. Adamo, J. Jaramillo, R. Gomperts, R. E. Stratmann, O. Yazyev, A. J. Austin, R. Cammi, C. Pomelli, J. W. Ochterski, R. L. Martin, K. Morokuma, V. G. Zakrzewski, G. A. Voth, P. Salvador, J. J. Dannenberg, S. Dapprich, A. D. Daniels, O. Farkas, J. B. Foresman, J. V. Ortiz, J. Cioslowski, D. J. Fox, Gaussian 09, Revision D.01, Gaussian, Inc., Wallingford CT, 2013.

SUPPORTING INFORMATION

Dye-modified silica-anatase nanoparticles for the ultrasensitive fluorogenic detection of the improvised explosive TATP in an air microfluidic device

Sindija Lapcinska,[a] Andrea Revilla-Cuesta,[b] Irene Abajo-Cuadrado,[b] José V. Cuevas,[b] Manuel Avella,[c] Pavel Arsenyan,[a]* Tomás Torroba[b]*

[a]*Latvian Institute of Organic Synthesis, Aizkraukles 21, LV-1006, Riga, Latvia.*

[b]*Department of Chemistry, Faculty of Science, University of Burgos, 09001 Burgos, Spain.*

[c]*Electron Microscopy Lab, IMDEA Materials Institute, Eric Kandel, 2, Tecnogetafe, 28906 Getafe (Madrid), Spain.*

1.- Characterization of SL-739

Figure S1: ^{1}H NMR (400 MHz, CD$_3$OD)
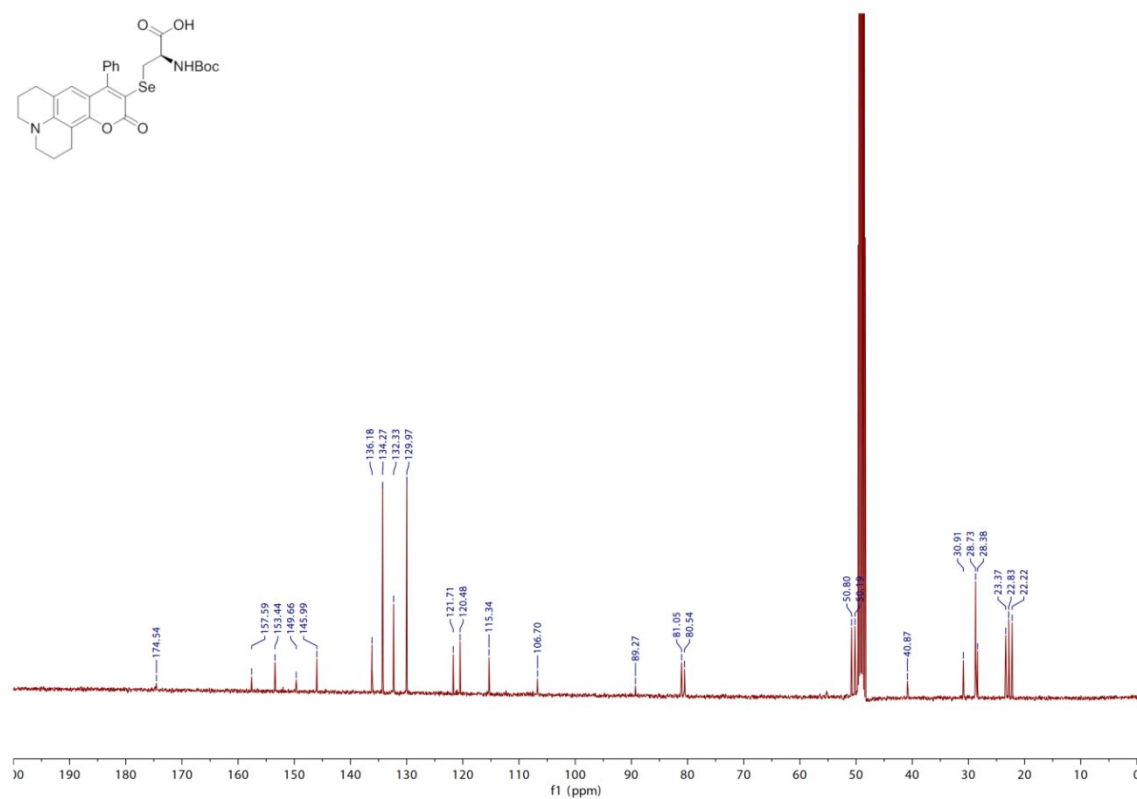
Figure S2: ^{13}C NMR (101 MHz, CD$_3$OD)
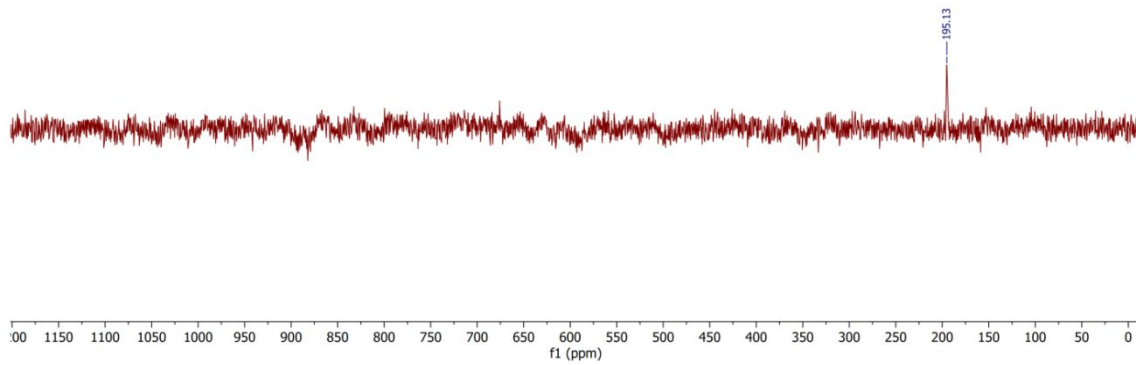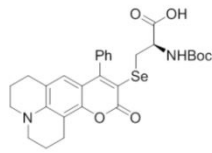
Figure S3: ^{77}Se NMR (76 MHz, CD$_3$OD)

HRMS_2020_02_429 884 (2.521) Cm (883:887-(852:869+906:916))   1: TOF MS ES+
                                                                                                                    1.08e7

HRMS_2020_02_429 884 (2.521) Cm (883:887-(852:869+906:916))   1: TOF MS ES+
                                                                                                                    6.97e6
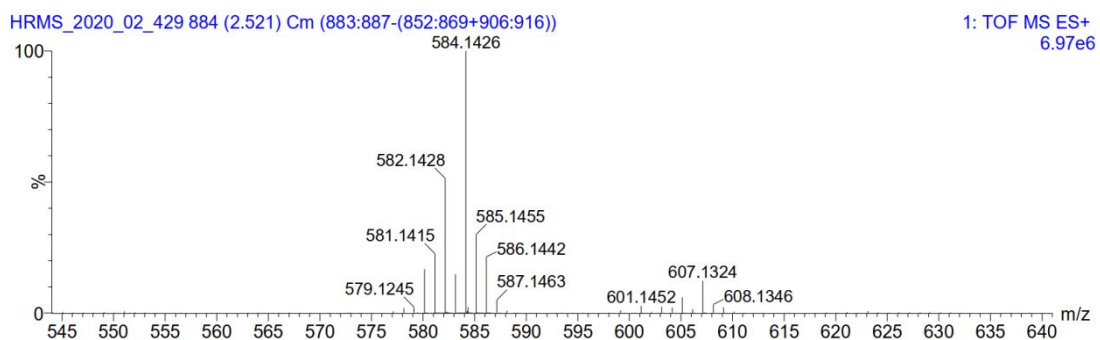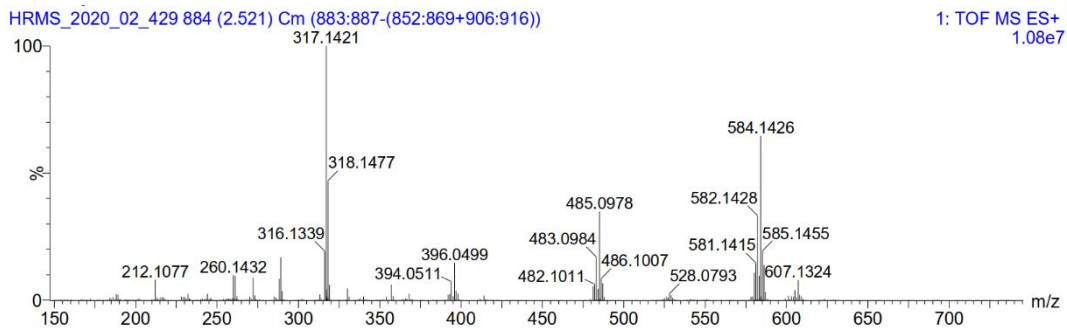
Figure S4: HRMS (ESI/Q-TOF)

2.- Solvatochromism tests

This test is performed at a concentration of $2*10^{-5}$ M and its objective is to select the most suitable solvent for subsequent tests. The solvents used in carrying out the solvatochromism tests are the ones shown in the following table:

1. H_2O	2. MeOH	3. DMSO
4. DMF	5. MeCN	6. Acetone
7. EtOAc	8. THF	9. $CHCl_3$
10. DCM	11. Toluene	12. Et_2O
13. Hexane	14. MCH	

Table S1. Solvents used in the solvatochromism test.

For each compound, the normalized absorbance, emission intensity and normalized emission spectra are shown; as well as UV images. The solvent chosen thanks to this test to perform the following ones must be miscible with water and present a fluorescence that allows to clearly observe increases, decreases and any other type of variation. UV and visible images are made for each compound right after the addition.
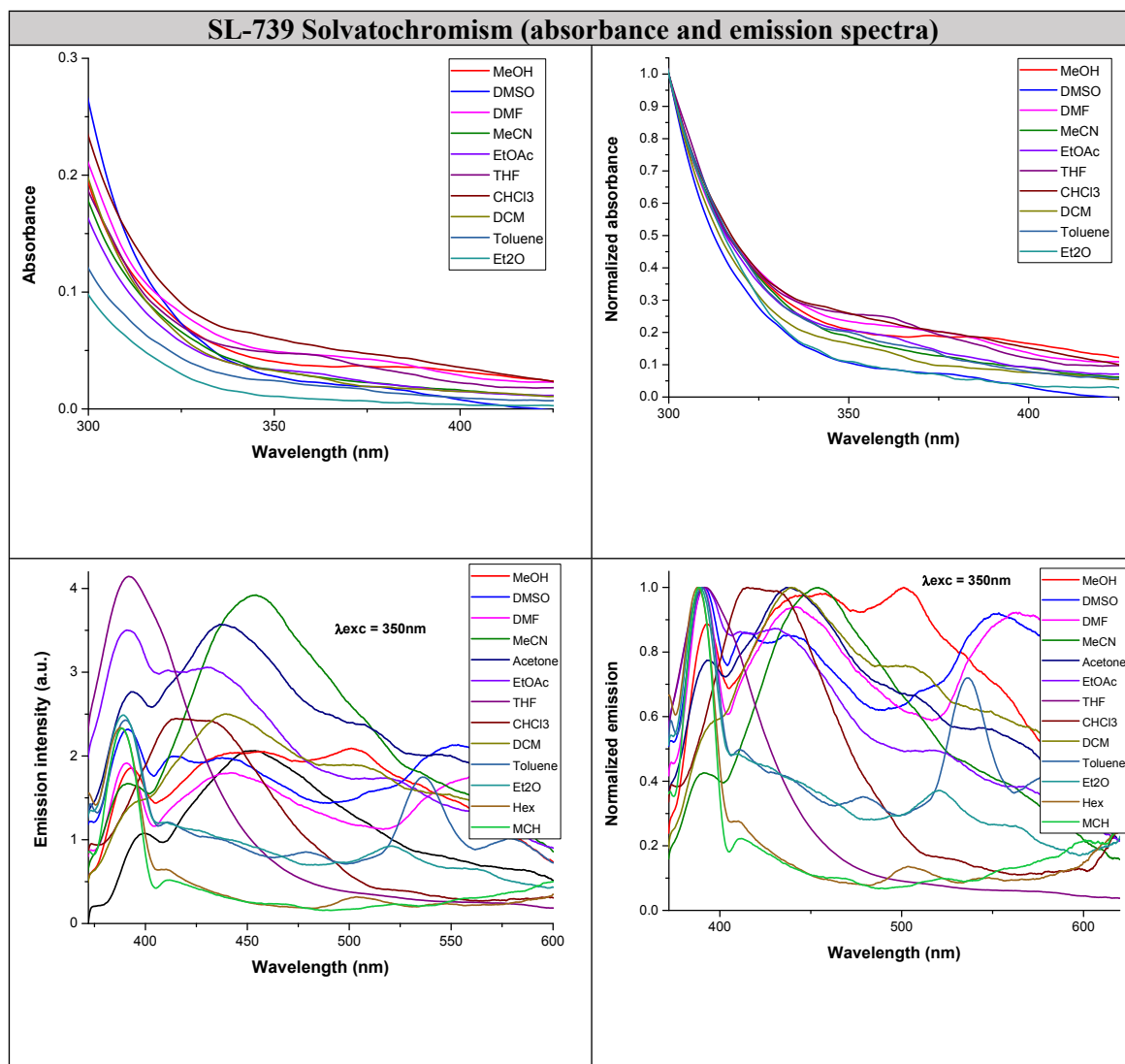

Table S2. SL-739 absorbance and emission spectra.

λ_{exc} = 350 nm. No clear displacement of the emission bands is observed as a function of the solvent.
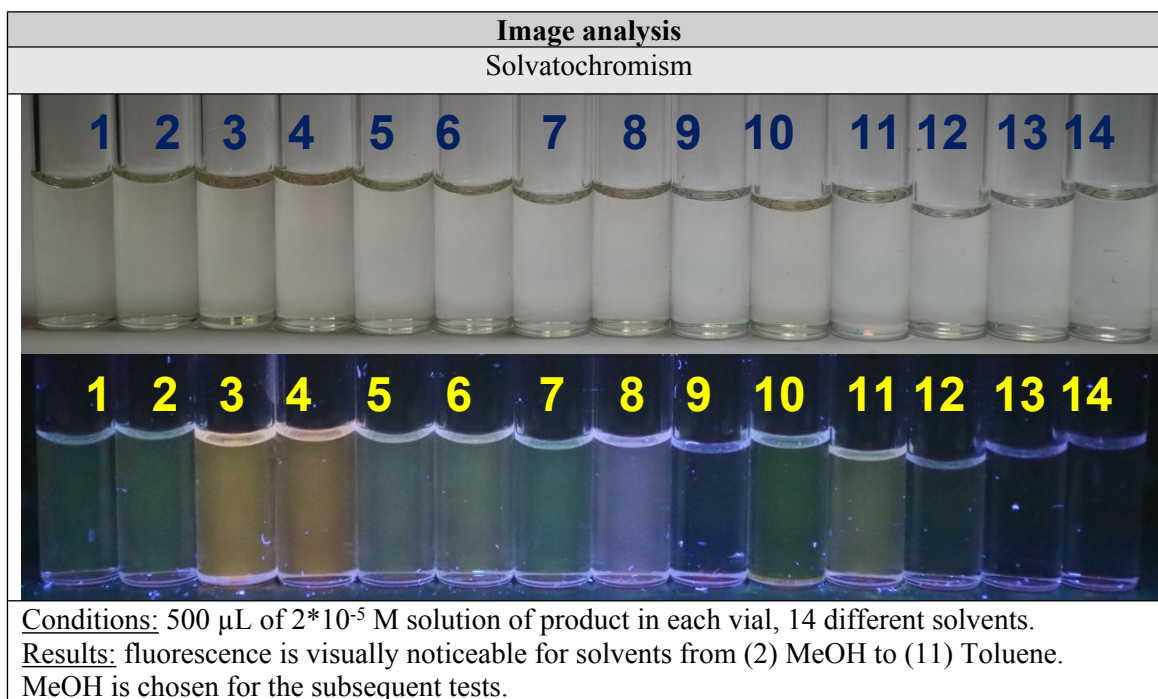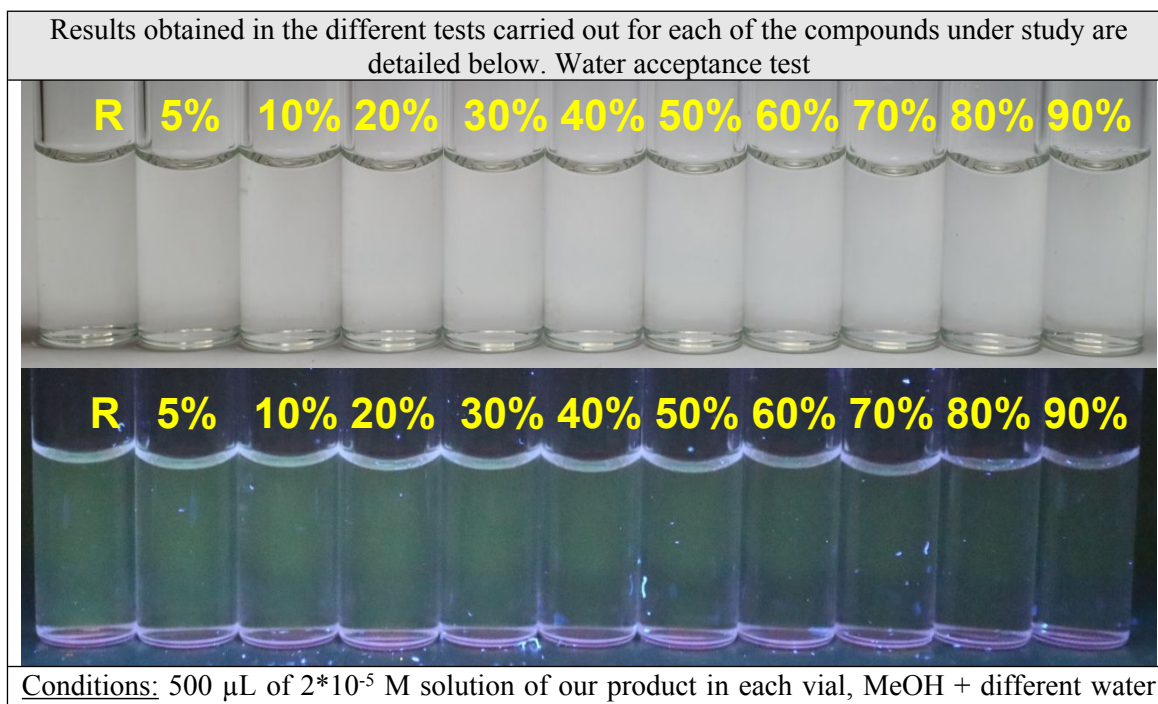
| **Image analysis** |
| Solvatochromism |
| |
| Conditions: 500 µL of 2*10⁻⁵ M solution of product in each vial, 14 different solvents.
Results: fluorescence is visually noticeable for solvents from (2) MeOH to (11) Toluene.
MeOH is chosen for the subsequent tests. |

Table S3. SL-739 solvatochromic tests.

3.- Water acceptance and pH tests

The water acceptance test consists of the preparation of 11 500µL vials of a 2*10⁻⁵ M solution of the compound, with increasing percentages of water (from 0% to 90%). The purpose of this test is to qualitatively determine the maximum water acceptance capacity of our product solution.

The pH test consists in subjecting our 2*10⁻⁵ M product solution to different pH conditions by adding 1M HCl, HEPES buffer solutions (pH 3.4, 4.8, 6.4, 7.4, 7.9 and 10.4) and 1M KOH in order to determine variations in fluorescence due to the effect of pH.

UV and visible images are made for each compound right after the addition.

| Results obtained in the different tests carried out for each of the compounds under study are detailed below. Water acceptance test |
| |
| Conditions: 500 µL of 2*10⁻⁵ M solution of our product in each vial, MeOH + different water |

percentages as solvent.
Results: a light green fluorescence can be seen. It disappears when a 60-70 water percentage is reached. The pH test is carried out with a water content of 70%.
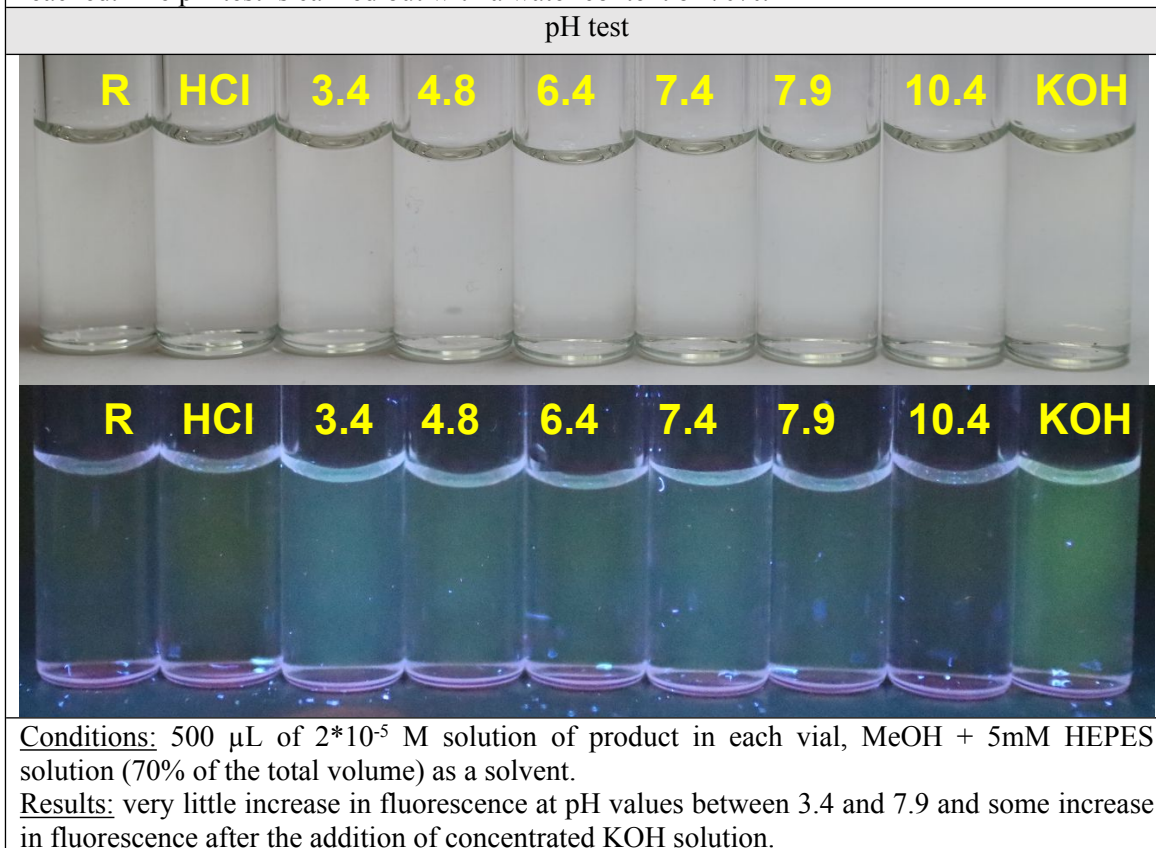
pH test

Conditions: 500 µL of $2*10^{-5}$ M solution of product in each vial, MeOH + 5mM HEPES solution (70% of the total volume) as a solvent.
Results: very little increase in fluorescence at pH values between 3.4 and 7.9 and some increase in fluorescence after the addition of concentrated KOH solution.

Table S4. SL-739 water percentage and pH tests.

4.- Ions test

This test consists of the addition of 1-2-4-8 eq of solutions corresponding to 11 different anions and cations to the $2*10^{-5}$ M solution of our compound to qualitatively observe and analyze variations in its fluorescence. The solutions of the different ions are prepared in water, so there is also a reference vial to which equivalent amounts of water are added. The solution of the product we are studying is carried out in the most suitable solvent (or solvent mixture) to correctly visualize changes in fluorescence. This solvent is selected, for each product, from the results obtained by the solvatochromism test. The ions solutions used in carrying out the test are the ones shown in the following table:

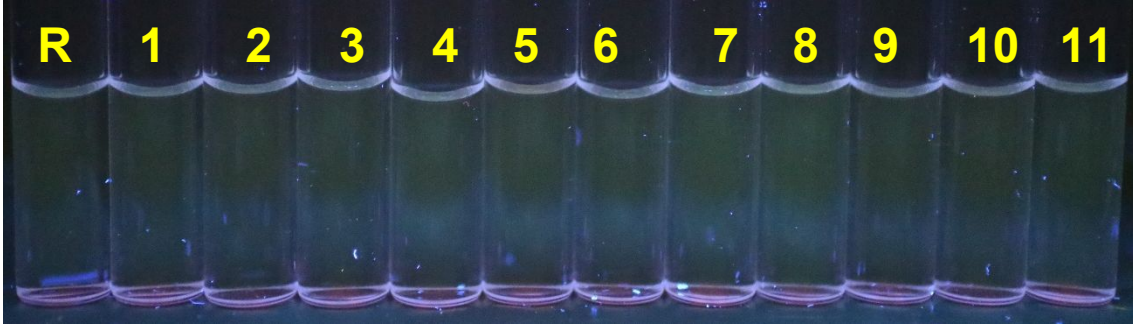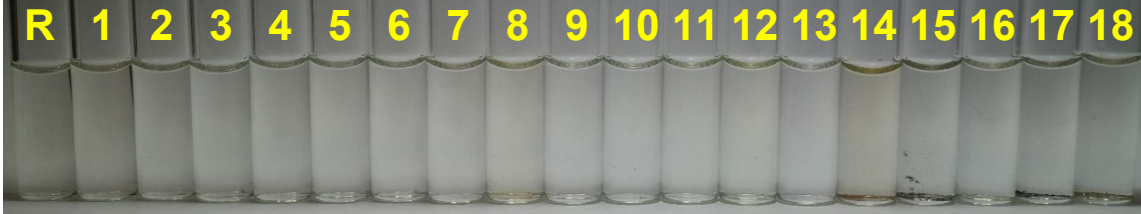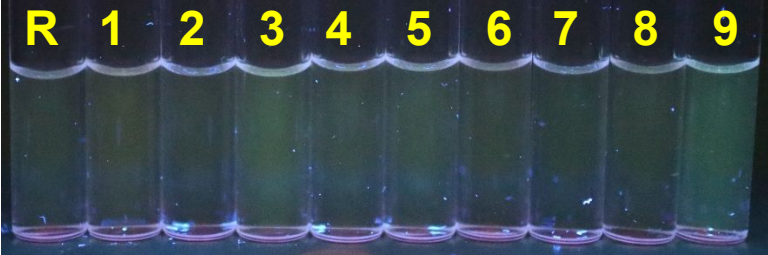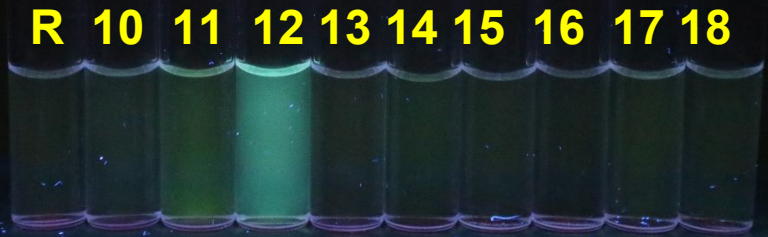| Anions			
1. F^-	2. Cl^-	3. Br^-	4. I^-
5. BzO^-	6. NO_3^-	7. $H_2PO_4^-$	8. HSO_4^-
9. AcO^-	10. CN^-	11. SCN^-	
Cations			
1. Ag^+	2. Ni^{2+}	3. Sn^{2+}	4. Cd^{2+}
5. Zn^{2+}	6. Pb^{2+}	7. Cu^{2+}	8. Fe^{3+}
9. Sc^{3+}	10. Al^{3+}	11. Hg^{2+}	12. Au^{3+}
13. Co^{2+}	14. Pd^{2+}	15. Ir^{3+}	16. Cu^+
17. Ru^{3+}	18. Pt^{2+}		

Table S5. Ion solutions used in the ion tests.

UV and visible images are made for the compound right after the addition. Anions tests

Conditions: 500 µL of 2*10⁻⁵ M solution of our product in each vial, MeOH as a solvent.
8eq of each anion solution have been added.
Results: there are no visible variations in the fluorescence of the product as a consequence of the addition of different anion solutions.

Cations tests

Conditions: 500 µL of 2*10⁻⁵ M solution of product in each vial, MeOH as a solvent.
8 eq of each cation solution have been added.
Results: A neat increase in fluorescence can be observed after the addition Au^{3+} solution (12).

Table S6. SL-739 ions tests.

5.- Work concentration

In order to choose an optimum concentration for a quantitative studio, the absorbance and fluorescence of the probe were checked to be linear while concentration changes are small (**Figure 1**). Studied in CHCl$_3$:MeOH (9:1 v:v):
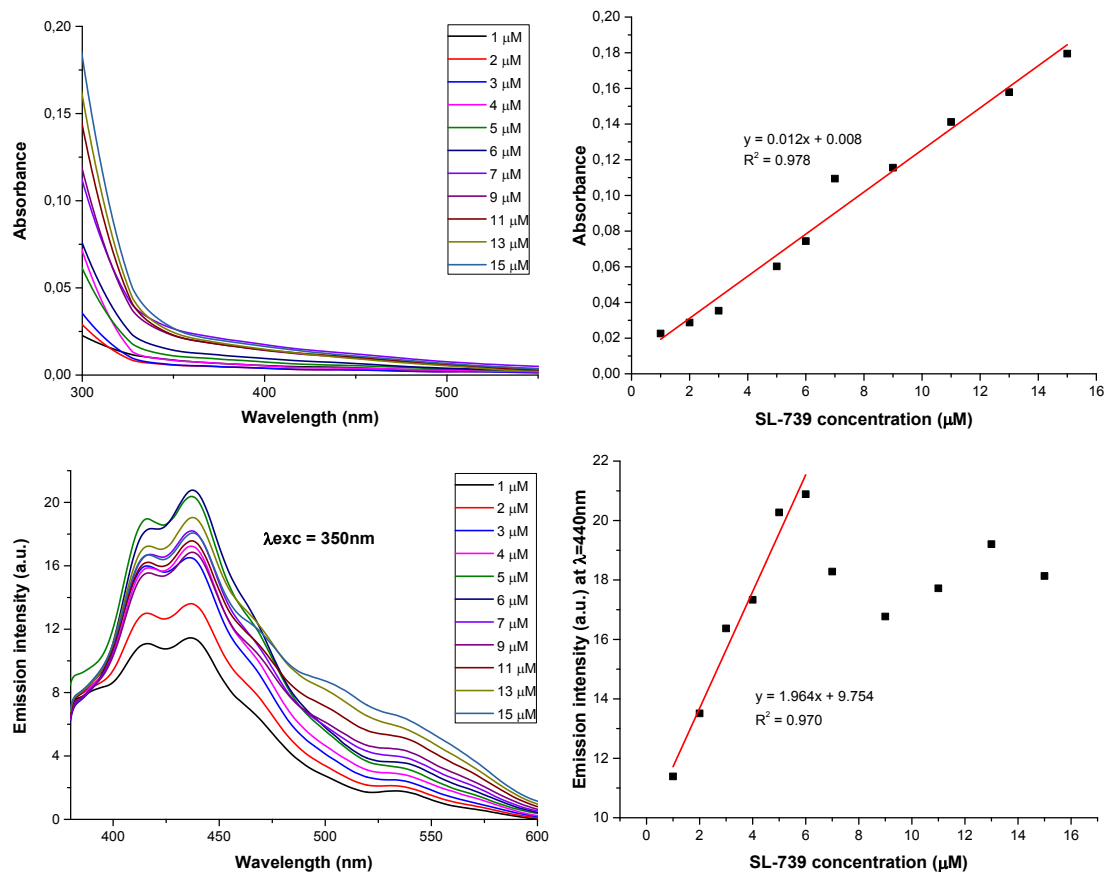

Figure S5. Absorbance (up) and fluorescence (down) of **SL-739** solution in CHCl$_3$:MeOH 9:1, under increasing concentrations of SL-739, λ_{exc} = 350 nm (down).

The work concentration ideally should stay at 0.1 of absorbance or less, to avoid inner filter effects, possible dynamic quenching or stacking processes. It implied a concentration below 7 μM**.** Taking the results into account, the chosen concentration was 2.5 μM, value around which the Lambert-Beer law (or pseudo-Lambert-Beer linear behaviour for fluorescence) was fulfilled.

6.- The recirculation system for TATP vapours

The recirculation system for the TATP vapours was designed. This system consisted of two plastic test tubes for centrifuge (Eppendorf) connected to each other. The first of them contained increasing amounts of TATP that were evaporated by

applying heat and was also connected to an air compressor that caused the vapours to circulate towards the second of the containers. This one contained SL-739 SiTiO$_4$ nanoparticles and its outlet hole connected again with the first Eppendorf in such a way as to produce a recirculation of the TATP vapours; as shown in the following images.

Figure S6. Complete recirculation system (left) designed for the experiment and close up view (right).

The calibration was performed in steady state, fixed quantities of TATP were vaporized in the presence of a sample containing 10 mg of SL-739 SiTiO$_4$ nanoparticles and the fluorescence increase was measured 10 minutes after the complete vaporization of each TATP sample.

Typical time for sublimation of TATP samples in the gas-solid experiments:

TATP (mg)	Sublimation time
0.032	1'41"
0.048	1'45"
0.083	2'14"
0.114	2'42"
0.158	3'10"
0.203	3'21"
0.247	3'57"
0.333	4'26"
0.483	5'03"
0.800	7'45"
1.000	11'23"
1.400	13'13"
2.100	19'37"

*10 minutes recirculation after evaporation of TATP samples.

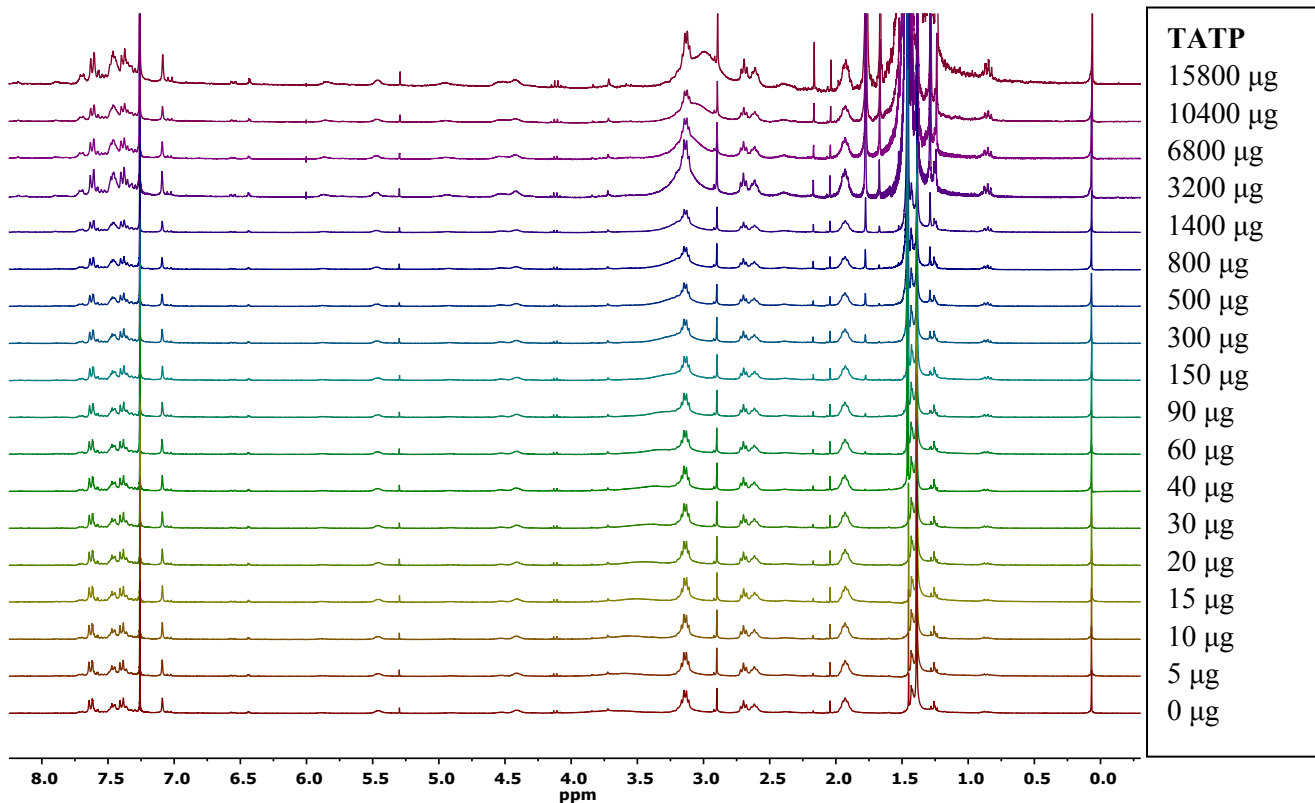*Table S7. Typical time for sublimation of TATP samples in the gas-solid experiments.*

7.- ^{1}H NMR Titrations of SL-739 with TATP and MCPBA

Figure S7: 1H NMR Titration of **SL-739** with TATP, 3 mg **SL-739** in 0.5 mL CDCl$_3$ as solvent, 5 µg to 15.8 mg TATP. Inset: Total amount of added TATP in each step.
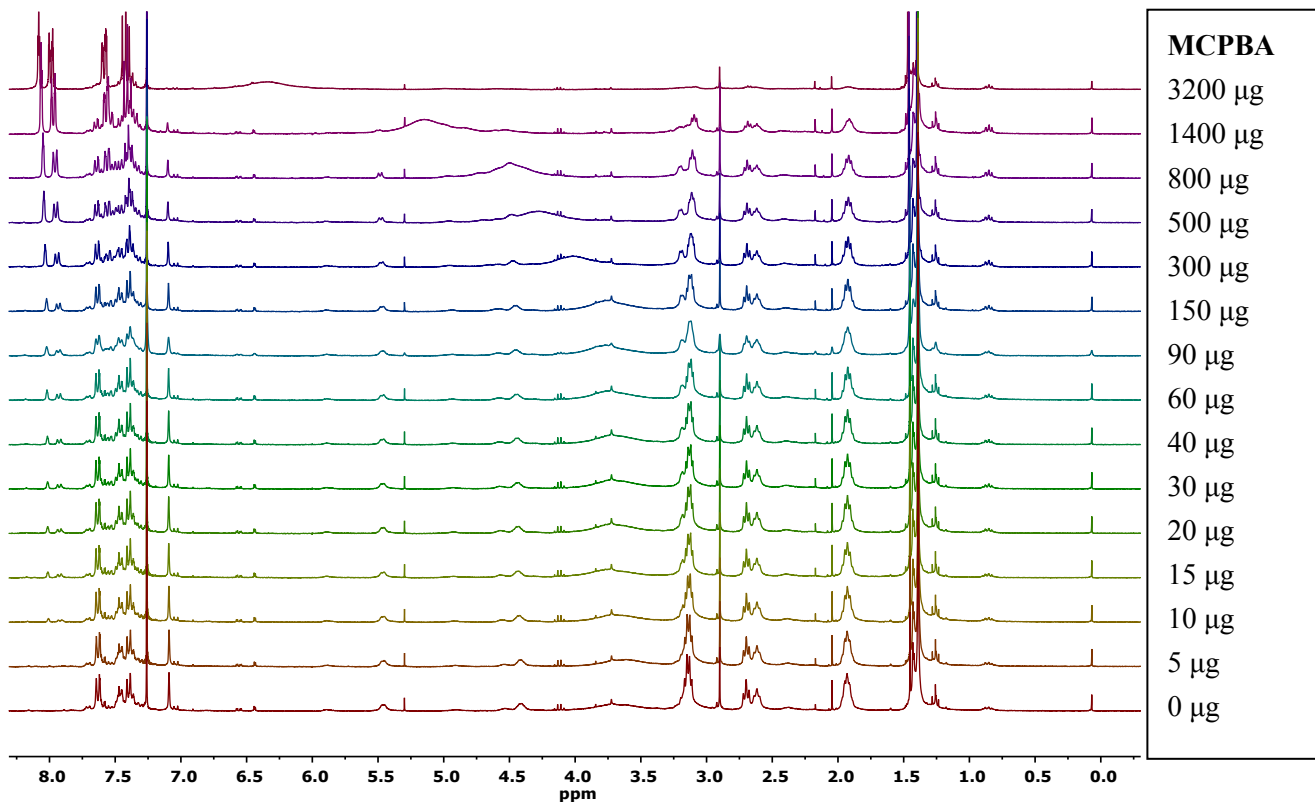

Figure S8: 1H NMR Titration of **SL-739** with MCPBA, 3 mg **SL-739** in 0.5 mL CDCl$_3$ as solvent, 5 µg to 3.2 mg TATP. Inset: Total amount of added MCPBA in each step.